Effect of Pressure and Temperature on Structural Stability of MoS2

ARTICLE *in* THE JOURNAL OF PHYSICAL CHEMISTRY C · FEBRUARY 2014

Impact Factor: 4.77 · DOI: 10.1021/jp410167k

10 AUTHORS, INCLUDING:

Ravhi S. Kumar
University of Nevada, Las Vegas
118 PUBLICATIONS **1,265** CITATIONS
SEE PROFILE

Jason L. Baker
University of Nevada, Las Vegas
12 PUBLICATIONS **17** CITATIONS
SEE PROFILE

Thomas Hartmann
University of Nevada, Las Vegas
82 PUBLICATIONS **827** CITATIONS
SEE PROFILE

Rama Venkat
University of Nevada, Las Vegas
53 PUBLICATIONS **198** CITATIONS
SEE PROFILE

THE JOURNAL OF PHYSICAL CHEMISTRY C

Article

pubs.acs.org/JPCC

Effect of Pressure and Temperature on Structural Stability of MoS_2

Nirup Bandaru,[†] Ravhi S. Kumar,*[,‡] Daniel Sneed,[‡] Oliver Tschauner,[‡,§] Jason Baker,[‡] Daniel Antonio,[‡] Sheng-Nian Luo,[∥] Thomas Hartmann,[⊥] Yusheng Zhao,[‡] and Rama Venkat[†]

[†]Department of Electrical and Computer Engineering, University of Nevada Las Vegas, Las Vegas, Nevada 89254, United States

[‡]Department of Physics & Astronomy and High Pressure Science and Engineering Center (HiPSEC), University of Nevada Las Vegas, Las Vegas, Nevada 89154, United States

[§]Department of Geology, University of Nevada Las Vegas, Las Vegas, Nevada 89154, United States

[∥]The Peac Institute of Multiscale Science, Jiang'an Campus, Sichuan University, Chengdu 610207, China

[⊥]Department of Mechanical Engineering, University of Nevada Las Vegas, Las Vegas, Nevada 89254, United States

ABSTRACT: The crystal structure and spectral properties of bulk MoS_2 were investigated at high pressures up to 51 GPa using a diamond anvil cell with synchrotron radiation in addition to high temperature X-ray diffraction and high pressure Raman spectroscopic analysis. While the crystal structure of MoS_2 is stable on increasing temperature, results of high pressure experiments show a pressure-induced isostructural hexagonal distortion to a $2H_a$-hexagonal $P6_3/mmc$ phase around 26 GPa as predicted by theoretical calculations reported earlier. The $2H_a$-hexagonal phase coexists with the ambient $2H_c$ phase up to 51 GPa, the highest pressure achieved in our experiments. The Raman data obtained in our high pressure experiments show consistent changes in the vibrational modes. Furthermore, the diffraction data obtained for the shocked MoS_2 to pressures 8 GPa is found to be structurally resilient.

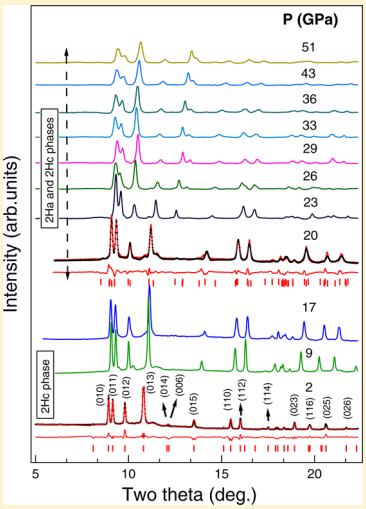

1. INTRODUCTION

The transition-metal dichalcogenides (TMDs) such as MoS_2 have attracted immense interest due to their unique structural, electronic, optical, and tribologic properties. MoS_2 is vastly used as a lubricant material in commercial industry including the aerospace industry. Also it is used as a catalyst for desulfurization of crude oil in refineries. Even though structurally MoS_2 resembles graphene, unlike graphene, which has low or no band gap (0 to 0.25 eV), MoS_2 exhibits finite band gap of 1.29 eV,[1−15] which makes it a promising material similar to Si for making a transistor and other electronic devices, which operate at room temperature. The crystal structure of MoS_2 is constituted by stacking a layer of transition metal (Mo) with two layers of chalcogens (S). Within this sandwich of three layers strong covalent bonds exist, but between the sandwiched layers weak van der Waals forces prevail, which upon application of shear force tend to slide over each other, thus giving rise to low friction and excellent dry lubricant properties. Because of the low friction and ability to withstand high impact pressures MoS_2 is widely used as a parent material for solid lubricants in industries, high vacuum, and space applications where liquid lubricants cannot be used. Further, MoS_2 serves multiple purposes when used as a supplement to liquid lubricants; it not only enhances the loading capability of the heavy machinery but also reduces any frictional losses due to surface contacts.[16] Furthermore, recent studies show that MoS_2 can be used as potential shock absorbing material, which has resulted in recent extensive studies on structural stability under the influence of high pressure.[17]

Under ambient pressure conditions, MoS_2 crystallizes in hexagonal structure similar to many compounds with general formula MX_2. High pressure characterization has proven to be an apt tool to improve the understanding of many physical properties of MoS_2, especially the tribologic ones. Both at ambient and under high pressure conditions, the structural stability of MoS_2 is very similar to those of carbonaceous MgB_2 and solid rare-gas (RG)-helium binary compounds, such as $Ne(He)_2$ and $Ar(He)_2$.[18,19] Even though many high pressure studies on crystal structure of molybdenbite (MoS_2) were performed up to about 39 GPa[20,21] and provide mixed interpretations about possible pressure induced transition, there is no confirmative study about detailing the effect of pressure on phase stability above 39 GPa. Furthermore,

Received: October 14, 2013
Revised: January 22, 2014

   dx.doi.org/10.1021/jp410167k | J. Phys. Chem. C XXXX, XXX, XXX−XXX

characterization using Raman spectroscopy under compression reported in the literature was limited up to only about 18 GPa,[22,23] and there is no experimental data on either crystal structure or Raman spectroscopy for pressures over 26 GPa. Hence, the aim of the present study is to examine the structural characteristics of MoS_2 under extreme pressure over a range of pressures from ambient to 51 GPa and correlate the phase transitions if they exist with Raman spectroscopy.

2. EXPERIMENTAL SECTION

2.1. X-ray Diffraction Experiments. High purity (99%) powders of MoS_2 with average particle size less than 2 μm were obtained from Sigma-Aldrich. The sample was loaded in a 150 μm hole of a symmetric-type diamond anvil high pressure cell in a rhenium gasket chamber with ruby grains for pressure measurement. The culet size of the diamonds was 300 μm, and the rhenium gaskets were indented to 50 μm for drilling. Neon was used as the pressure transmitting medium. High pressure experiments were performed at the high-resolution powder diffraction beamline at Sector 16 μ_B−D of HPCAT at the Advanced Photon Source. A monochromatic X-ray beam from a double crystal branching monochromator was focused to a size of 5 × 15 μm using Kickpatrick−Baez mirrors. A MAR-345 imaging plate was used in the experiments to obtain high quality powder diffraction patterns from the samples. An incident monochromatic X-ray beam of wavelength of λ = 0.424603 Å for the experiments was used. The detector distance was calibrated by collecting a CeO_2 standard. Because of the weak X-ray scattering signal from the sample, longer exposure time of about 5 min was necessary to improve the signal-to-noise ratio. The Debye−Scherrer rings recorded by the MAR imaging plate were then integrated using the Fit2D software to obtain one-dimensional intensity versus diffraction angle plot.[24] The diffraction patterns were analyzed with JADE 7.0 commercial software program and Rietica (LHPM) software package for obtaining structural information.[25] The pressure at the sample site was determined by measuring the shift of the R1 fluorescence line of ruby with an online system at HPCAT and fitting with the standard ruby pressure scale.[26] Initial set of experiments were conducted at room temperature at high pressures in the range of 0 to 51 GPa.

At the conclusion of the high-pressure X-ray diffraction run, an additional set of experiments were run with the sample heated (resistive heating) to a series of selected temperatures in the range of 100 to 500 °C with the pressure held constant at 51 GPa. This was performed to check the combined effect of high pressure and temperature together on the crystal structure at the highest pressure achieved in our experiments. The diffraction data were collected for the four temperature points: ambient, 60, 90, and 120 °C.

Additionally, a separate run was conducted to understand only the effect of temperature on the structural stability. High temperature X-ray diffraction measurements at ambient pressure were performed at UNLV using a Bruker D8 Advance Vario high-resolution powder X-ray diffractometer with Cu Kα_1 incident radiation (λ = 1.54063 Å). The sample was enclosed in a capsule at ambient atmosphere pressure and heated up to 500 °C. Diffraction patterns were collected at six different temperatures: 25 (ambient), 100, 200, 300, 400, and 500 °C under air. The diffraction patterns were then analyzed by the same software programs used for analysis of the data in the pressure experiments carried out at HPCAT.

For the shock experiments $MoS_2$was compressed into a recovery chamber with rhenium driver and flyer. A single stage light gas gun was used to launch the flyer onto the target chamber. Shock pressure in the rhenium driver was 28 GPa, and peak shock pressure in the MoS_2 sample was estimated to 8 GPa by impedance match in a reverberative shock compression. We have used the reported isothermal bulk modulus and K_o'[20] for estimating the material specific impedance parameters C and S. The recovery chamber remained intact during the experiment. High-resolution powder X-ray diffraction was performed on the recovered sample at Sector 16 μ_B−D of HPCAT at the Advanced Photon Source. A MAR-345 imaging plate was used in the experiments to obtain high quality powder diffraction patterns from the samples. An incident monochromatic X-ray beam of wavelength of λ = 0.424603 Å for the experiments was used. The detector distance was calibrated by collecting a CeO_2 standard similar to high-pressure diffraction experiments.

2.2. Raman Spectroscopy. Raman experiments were performed with an Ar-ion laser using an excitation wavelength of 514.5 nm operating at 100 mW. The spectra through the diamond anvil cell were recorded with an ISA Jobin-Yuvon U1000 double-grating spectrometer equipped with a charge coupled device (CCD) detector (ISA SpectrumOne) with an effective resolution of 1 cm^{-1}. The sample was loaded in a 150 μm hole of a Merrill−Bassett-type diamond anvil high pressure cell in a stainless steel gasket chamber with ruby grains for pressure measurement. The culet size of the diamonds was 300 μm, and the steel gaskets were indented to 50 μm for drilling. A 4:1 methanol and ethanol mixture was used as the pressure transmitting medium. Pressure at the sample site was determined by the standard ruby fluorescence method. The pressure dependence of the active vibrational Raman modes of MoS_2 was monitored upon increasing pressure at ambient temperature.

3. RESULTS AND DISCUSSION

3.1. Structural Stability at High Temperatures. Powder X-ray diffraction patterns for MoS_2 samples at ambient and at temperatures in the range of 100 to 600 °C are shown in the Figure 1. At ambient conditions, MoS_2 crystallizes in the hexagonal space group $P6_3/mmc$. The XRD patterns collected showed the sample in a single phase and the lattice parameter were refined to a = 3.159(8) Å and c = 12.298(3) Å. From Figure 1, it is clear that upon heat treatment, the relative 2θ position of the diffraction peaks remained virtually unchanged with respect to application temperatures up to 500 °C. The additional weak peaks (less than 5%) in the temperature-dependent XRD pattern may be due to surface oxidation of the sample since the predominant lines showed no changes upon increasing temperature. This leads us to the conclusion that the crystal structure of MoS_2 is stable up to 500 °C under ambient pressure conditions, which is in good agreement with the earlier work.[26] Further, it was noticed that for temperatures above 500 °C MoS_2 oxidizes and decomposes into MoO_3 and SO_2. It is noted that the intensity of the (002) peak (~13° 2θ) decreases continuously with increasing temperature due to increasingly larger temperature factors. As expected, increasing temperature produced a larger lattice parameter and expanded unit cell volumes. Further, it was observed that the initial Wyckoff's positions of Mo and sulfur atoms at 2c and 4f, respectively, remained unperturbed with an increase in the temperature up to 500 °C.

dx.doi.org/10.1021/jp410167k | J. Phys. Chem. C XXXX, XXX, XXX−XXX

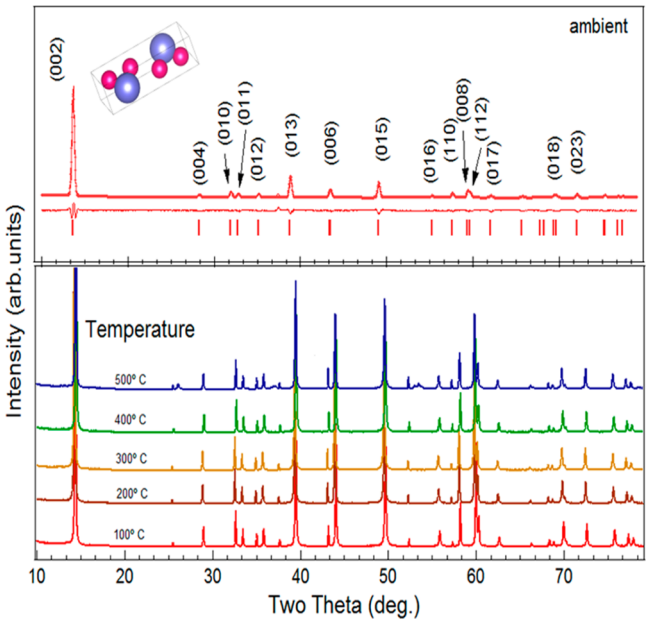

Figure 1. X-ray diffraction patterns of MoS_2 at ambient and elevated temperatures. The top panel shows the measured and the calculated MoS_2 pattern using Rietveld structure refinement at ambient temperature. The unit cell is displayed; the large solid spheres represent Mo, and smaller spheres represent S atoms.

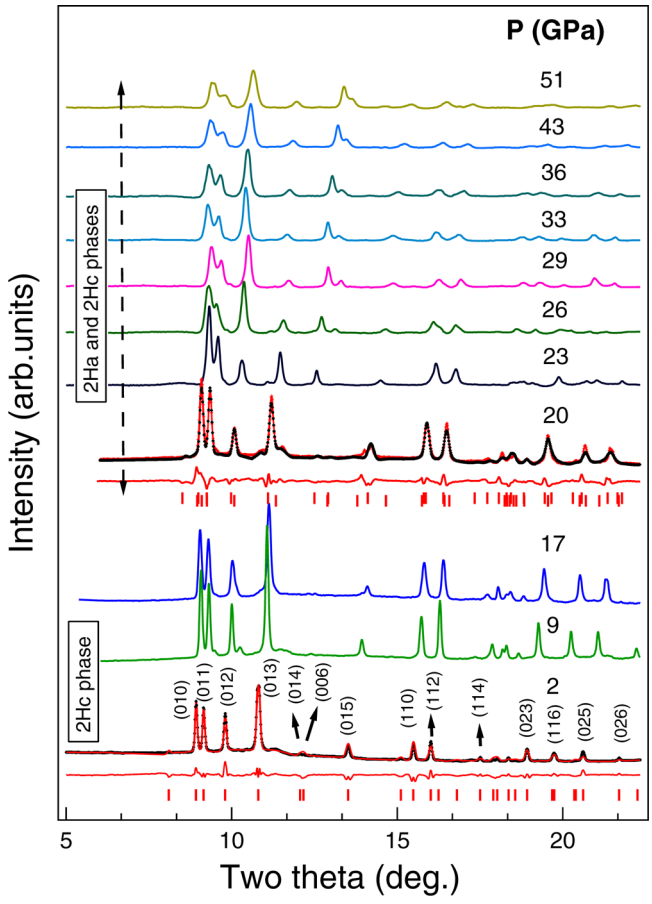

Figure 2. Representative synchrotron powder X-ray diffraction patterns at various pressures for MoS_2. The calculated (continuous line; symbols, data) difference and phase markers obtained from Rietveld refinement are plotted for 2 and 20 GPa.

3.2. Pressure-Induced Structural Transitions. The evolution of diffraction patterns with increasing pressure is shown in Figure 2. As displayed in Figure 2, the diffraction patterns look similar up to 23 GPa except for a gradual shift in peak position toward larger 2θ values caused by decreasing lattice planes. However, for pressures around 17 GPa, a new line, next to (006) lattice plane, emerges corresponding to d-spacing of 1.774 Å (13.75° 2θ). The emergence of this line occurs along with the increase in intensities of the (102) lattice plane and drop in the intensities of the (103) and (105) lines, respectively. Further, beyond 26 GPa it is found that the intensities of the major peaks located at 9.2° 2θ and 9.47° 2θ, and d_{hkl} =2.647 and 2.572 Å, respectively, decreased noticeably. In addition, the intensity of the diffraction peak (102) increased consistently with increasing pressure up to 51 GPa. These changes may suggest the presence of another phase, which emerges around 17 GPa, in addition to the parent structure ($2H_c$–hexagonal, $P6_3/mmc$). These changes are also observed in previous studies[20,21] but are not conclusive to be explained by a structural transition. To the best of our knowledge, there are no previous conclusive experimental reports on the nature of the MoS_2 crystal structure under extreme pressure conditions above 26 GPa. Even though a possible electronic or structural phase transition with partial distortion around the same pressure point is suspected by Aksoy et al., they did not provide any further details. Later, a theoretical study on structural stability of MoS_2 by Hromadova et al. indicated a possible structural distortion to a $2H_a$-type hexagonal phase.[21] Structural refinement was carried at low pressures, assuming presence of only $2H_c$-type structure, with Mo and S atoms positioned at 2(b) and 4(f) (z = 0.6118) Wyckoff's positions, respectively. However, for pressures around 20 GPa and beyond, a two phase fitting was carried out as suggested in ref 21. The obtained refined atomic positions for Mo and S atoms involving both for the phases, $2H_c$ and $2H_a$, are 2(b), 4(f) (z = 0.6350(1)) and 2(c), 4f (z = 0.9155(7)), respectively. These results presented in Table 1 are very much in agreement with ref 21. As most of the other diffraction peaks corresponding to the parent phase ($2H_c$–hexagonal structure, $P6_3/mmc$) survived during compression, possible presence of mixed phase region is observed. Our results agree well with the structural distortion predicted by the ab initio calculations.[21] Hence, from our observations it can be inferred that under high pressure the atomic positions experience a partial distortion, in particularly Mo atoms, thus suggesting the presence of isostructural $2H_a$ phase due to change in Wyckoff's position of Mo atoms from 2(c) to 2(b) under high pressure. Further, on the basis of previous theoretical studies performed by Gundelli et al.[28] on similar compounds such as FeS_2, the suggested pressure induced phase transitions are very much dependent upon the c/a ratio and the chalcogen–metal–chalcogen bond angle. Since MoS_2 has a high c/a ratio and bond angle less than 90°, we expect pressure-induced phase transitions at elevated pressures.

Our analysis of high pressure X-ray diffraction data assuming presence of the $2H_c$ crystal structure resulted in successful indexing of almost all diffraction peaks in the X-ray pattern. Lattice parameters as a function of pressure are shown in Figure 3. It is observed from Figure 3 that the initial rate of change of lattice constants, $(d(c/c_0)/dp)$ and $(d(a/a_0)/dp)$ is rapid and gradually slows down with the increase in pressure up to 23 GPa. In fact, rate of change of lattice parameter, c is higher than

dx.doi.org/10.1021/jp410167k | J. Phys. Chem. C XXXX, XXX, XXX–XXX

Table 1. Rietveld Refinement Parameters at 2 and 20 GPa for MoS_2

	2 (GPa)	20 GPa	
	$2H_c$	$2H_c$	$2H_a$
space group	$P6_3/mmc$	$P6_3/mmc$	$P6_3/mmc$
a (Å)	3.1504(6)	3.0389(3)	3.048(6)
c (Å)	12.016(4)	11.101(4)	10.410(5)
volume (Å^3)	103.2(8)	88.7(8)	83.79(5)
Mo (x,y,z)	(1/3,2/3,1/4)	(1/3,2/3,1/4)	(0,0,1/4)
S (x,y,z)	(1/3,2/3,0.6118(9))	(1/3,2/3,0.6350(1))	(1/3,2/3,0.9155(7))
R_{wp}	3.4%	5.5%	

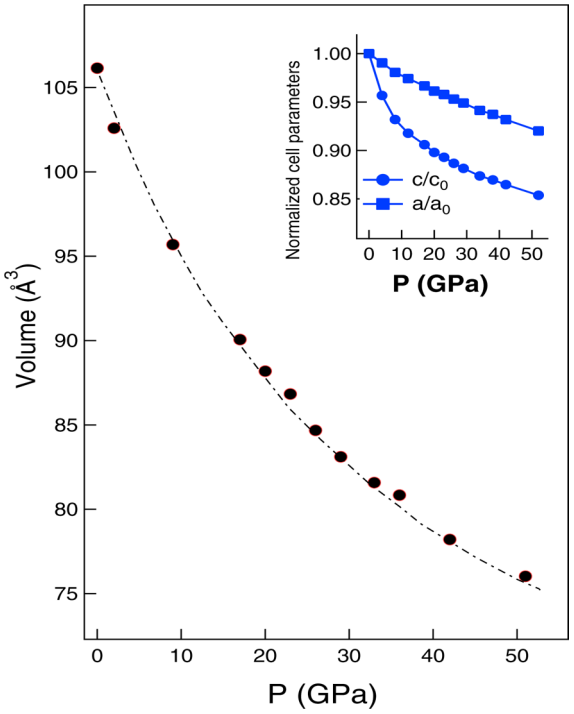

Figure 3. Pressure versus volume plot for MoS_2. The dotted line is the fit with Birch–Murnaghan equation of state. The inset shows the variation of cell normalized parameters as a function of pressure. The error bars are smaller than the size of the symbols.

that of a, which suggests that the nature of compression is anisotropic along the c axis. However, around pressure point 26 GPa, interestingly, we observe significant change in the evolution of lattice parameters, particularly lattice constant a. The sign of the slope changes from negative to positive and thus indicating an increase in a at that point. Above 26 GPa, the slope of the path traced by the parameter a is different and lower than the initial slope, whereas the rate of change of lattice constant c increases rapidly for pressures starting from 26 GPa and hence suggesting a sharp decrease in lattice parameter c. Further, since the change in lattice constants at various pressure points is beyond their calculated individual maximum error bars (a = ±0.0001 Å and c = ±0.001 Å), the dispersion in data clearly implies phase transition. The aforementioned inferences are very much consistent with the earlier report[21] and strongly suggest the presence of mixed phase region, that is both $2H_c$ and $2H_a$, for pressure beyond 17 GPa, with $2H_c$ being the dominant phase.

Assuming the hexagonal $2H_c$ phase for all the pressure range 0–51 GPa, the unit cell volume as a function of pressure was calculated and is shown in Figure 3. It is observed that the unit cell volume decreases gradually upon increase in pressure, and we did not observe any volume collapse. A third order Birch–Murnaghan equation of state (EOS) was used for fitting the P–V data. The maximum error between the calculated and observed pressure values is 0.66 and 1.06 GPa for third and second order Birch–Murnaghan EOS fits, respectively. The obtained third and second order bulk module are B_0 = 70 ± 5 GPa (B'_0 = 4.5) and B_0 = 79.5 ± 2 GPa (B'_0 = 4.0). The difference between the calculated second and third order bulk modulus can be ascribed due to fixed B'_0 in the case of the former. The bulk modulus obtained in our studies agrees well with the bulk modulus reported by Resul Aksoy et al.[20] We have further collected X-ray diffraction patterns for MoS_2 locked at the highest pressure (51 GPa) for four different chosen temperatures (ambient, 60, 90, and 120 °C), and the results show no significant changes at HP-HT conditions. No further high pressure transitions were observed.

3.3. Dynamic Compression and Static Compression. MoS_2 is reported to be an excellent shock absorber.[17] In order to test the shock behavior we have compared the X-ray diffraction data collected for the shocked MoS_2 sample with static high pressure data and previous reports. We have observed no structural deformation on MoS_2 subjected to shock pressure up to 8 GPa. From the post-data analysis, we noticed that the structure remains stable and that cell parameters agree well with the reported data.[17]

3.4. Raman Spectroscopy. MoS_2 belongs to D^4_{6h} ($P6_3/mmc$) space group and is iso-symmorphic. Since MoS_2 is a nonlinear molecule and there are six atoms per unit cell (N = 6); hence, $3N - 6 = 12$ normal modes of vibration exist at the center of hexagonal Brillouin zone and are given by the following equation:

$$\Gamma = A_{1g} + 2A_{2u} + 2B_{2g} + B_{1u} + E_{1g} + 2E_{1u} + 2E_{2g} + E_{2u} \quad (1)$$

Of the aforementioned 12 modes, A_{1g}, E_{1g}, E^1_{2g}, and E^2_{2g} are Raman active, and the remaining are infrared absorption and acoustic. In plane, E^1_{2g}, and out of plane, A_{1g}, are the two most commonly studied internal molecular modes under pressure. The two external modes, namely, rigid modes E_{1g} and E^2_{2g}, are associated with movement of the layers. In the present work, we limit our study to two internal modes of vibrations. Under ambient pressure conditions, the energy corresponding to the two internal lattice vibrations are $E^{(1)}_{2g}$ at 383.4 cm^{-1} and A_{1g} at 408.5 cm^{-1}, respectively. The observed pressure dependence of these modes is shown in Figure 4. It can be seen that both $E^{(1)}_{2g}$ and A_{1g} modes red shift with increase in applied hydrostatic pressure. Further, from the data it can be inferred that the initial rate of shift of vibrational frequencies is rapid with pressure, but for pressures above 5 GPa, the rate of

dx.doi.org/10.1021/jp410167k | J. Phys. Chem. C XXXX, XXX, XXX–XXX

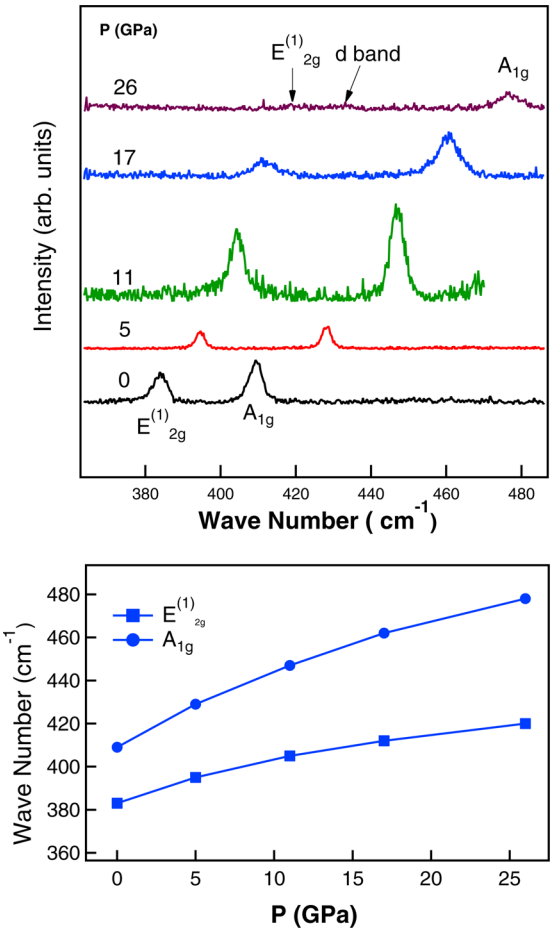

Figure 4. Pressure dependence of the Raman active vibrational frequencies A_{1g} and $E^{(1)}_{2g}$.

increase slows down. Moreover, it is noticed from the plot that both the modes more or less vary linearly with pressure and are in good agreement with the data of Bangall et al.[23] and Sugai et al.[22]

Interestingly for pressures between 17 to 26 GPa, when both the phases, $2H_c$ and $2H_a$, coexist, one of the Raman modes, i.e., in plane, $E^{(1)}_{2g}$, significantly peak broadens along with reduced intensity. Further, in the background we notice a new peak emerges, corresponding to 432 cm^{-1} wavenumber, and we strongly suspect this is due to the presence of another phase, $2H_a$, along with the original $2H_c$ phase. Also recent studies by Tsachi Livneh et al.[29] also confirmed the existence of this new peak, namely, d band between the 19 to 31 GPa pressure range. However, A_{1g} out of plane Raman mode red shifts systematically as expected[22,23] with significant reduction in the peak intensity, accompanied by the peak broadening. From these observations, it can be inferred that the material MoS_2 has two phases between 17 to 26 GPa, with $2H_c$ being the dominant one. This observation of a possible structural distortion is consistent with the results of X-ray diffraction spectrum under high pressure experiment.

4. SUMMARY AND CONCLUSIONS

In situ high pressure powder X-ray diffraction experiments using synchrotron radiation were carried out up to 51 GPa on MoS_2, and the cell parameters were obtained as a function of pressure. In addition, diffraction experiments were performed as a function of temperature in the range of 25 to 500 °C, and samples were shocked to study the crystal structure stability. On the basis of our experiments, we conclude the following:

- The $2H_c$ hexagonal phase of MoS2 is very stable up to 500 °C.
- MoS_2 undergoes a pressure-induced structural distortion around 26 GPa from the $2H_c$ phase to a $2H_a$-type hexagonal phase as predicted by theoretical simulations. Both phases coexist up to 51 GPa.
- From the Raman spectroscopy, we notice that in the background, a new mode, namely, d band, pertaining to $2H_a$ phase structure emerges next to the already existing in plane vibrational mode $E^{(1)}_{2g}$ between 17 and 26 GPa, which further reinforces our observation in high-pressure diffraction experiments.
- Structural data on shocked MoS_2 show no significant changes, which means that MoS_2 is a good shock absorber, consistent with earlier reports.

AUTHOR INFORMATION

Corresponding Author

*(R.S.K.) E-mail: ravhi@physics.unlv.edu.

Notes

The authors declare no competing financial interest.

ACKNOWLEDGMENTS

The authors acknowledge Sergey Tkachev and COMPRESS gas loading facility at Sector 13, APS. The authors also acknowledge Michael Pravica for Raman experiments. Work at UNLV is supported by UNLV (ALC), funded by U.S. Department of Energy Award DESC0005278. Portions of this work were performed at HPCAT (Sector 16), Advanced Photon Source (APS), and Argonne National Laboratory. HPCAT is supported by DOE-BES, DOE-NNSA, NSF, and the W.M. Keck Foundation. APS is supported by DOE-BES, under Contract No. DE-AC02-06CH11357.

REFERENCES

(1) Lee, P. A. *Physics and Chemistry of Materials with Layered Structures: Optical and Electrical Properties*; D. Reidel Publishing Company: Dordrecht, Netherlands, 1976; Vol. *4*.

(2) Kasowski, R. V. Band Structure of MoS_2 and NbS_2. *Phys. Rev. Lett.* **1973**, *30*, 1175−1178.

(3) Mattheis, L. F. Band Structures of Transition-Metal-Dichalcogenides Layer Compounds. *Phys. Rev. B* **1973**, *8*, 3719−3740.

(4) Miremadi, B. K.; Colbow, K.; Morrison, S. R. A New Magnetic Lubricating Material from MoS_2. *J. Appl. Phys.* **1997**, *82*, 2636−2639.

(5) Le Mogne, T.; Donnet, C.; Martin, J.; Tnock, A.; Millard- Pinard, N. Nature of Super-Lubricating MoS_2 Physical Vapor Deposition Coatings. *J. Vac. Sci. Technol. A* **1994**, *12*, 1998−2004.

(6) Spalvins, T. A Review of Recent Advances in Solid Film Lubricants. *J. Vac. Sci. Technol. A* **1987**, *5* (2), 212−219.

(7) Singer, I. L.; Pope, L.; Fehrenbacher, L.; Winer, W. New Materials Approaches to Tribiology, Theory and Applications. *Mater. Res. Soc. Symp. Proc.* **1989**, 215−219.

(8) Li, T. S.; Galli, G. L. Electronic Properties of MoS_2 Nanoparticles. *J. Phys. Chem. C* **2007**, *111*, 16192−16196.

(9) Lebegue, S.; Eriksson, O. Electronic Structure of Two-Dimensional Crystals from ab Initio Theory. *Phys. Rev. B* **2009**, *79* (11), 115409−115412.

(10) Coehoom, R.; Hass, C.; De Groot, R. A. Electronic Structure of $MoSe_2$, MoS_2, and WSe_2. I. Band-Structure Calculations and Photoelectron Spectroscopy. *Phys. Rev. B* **1987**, *35* (11), 6195−6202.

dx.doi.org/10.1021/jp410167k | *J. Phys. Chem. C* XXXX, XXX, XXX−XXX

(11) Arslan, E.; Bulbil, E.; Efeoglu, I. The Structure and Tribological Properties of MoS_2-Ti Composite Solid Lubricants. *Tribol. Trans.*. **2004**, *47*, 218−226.
(12) Liang, W. Y. Optical Anisotropy in Layer Compounds. *J. Phys. C: Solid State Phys.* **1973**, *6*, 551−565.
(13) Zong, X.; Yan, H.; Wu, G.; Ma, G.; Wen, F.; Wang, L.; Li, C. Enhancement of Photocatalytic H_2 Evolution on CdS by Loading MoS_2 as Cocatalyst Under Visible Light Irradiation. *J. Am. Chem. Soc.* **2008**, *130*, 7176−7177.
(14) Wilson, J. A.; Yoffe, A. D. The Transition Metal Dichalcogenides Discussion and Interpretation of the Observed Optical, Electrical and Structural Properties. *Adv. Phys.* **1969**, *18*, 193−335.
(15) Boker, T.; Severin, R.; Muller, A.; Janowitz, C.; Manzke, R.; Vob, D.; Kruger, P.; Mazur, A.; Pollmann, J. Band Structure of MoS_2, $MoSe_2$, and α-$MoTe_2$: Angle-Resolved Photoelectron Spectroscopy and ab Initio Calculations. *Phys. Rev. B* **2001**, *64*, 235305−235315.
(16) Bollinger, M. V.; Jacobsen, K. W.; Norskov, J. K. Atomic and Electronic Structure of MoS_2 Nanoparticles. *Phys. Rev. B* **2003**, *67*, 085410−085427.
(17) Zhu, Y. Q.; Sekine, T.; Li, Y. H.; Fay, M. W.; Zhao, Y. M.; Poa, C. H. P.; Wang, W. X.; Roe, M. J.; Brown, P. D.; Fleischer, N.; Tenne, R. Shock-Absorbing and Failure Mechanisms of WS_2 and MoS_2 Nanoparticles with Fullerene-Like Structures Under Shock Wave Pressure. *J. Am. Chem. Soc.* **2005**, *127* (46), 16263−72.
(18) Tschauner, O.; Errandonea, D.; Serghiou, G. Possible Superlattice Formation in High-Temperature Treated Carbonaceous MgB_2 at Elevated Pressure. *Phys. B: Condens. Matter* **2006**, *371* (1), 88−94.
(19) Cazorla, C.; Errandonea, D.; Sola, E. High-Pressure Phases, Vibrational Properties, and Electronic Structure of $Ne(He)_2$ and $Ar(He)_2$: A First-Principles Study. *Phys. Rev. B* **2009**, *80*, 064105−064118.
(20) Resul, A.; Yanzhang, M.; Emre, S.; Chyu, M. C.; Atila, E.; White, A. X-ray Diffraction Study of Molybdenum Disulfide to 38.8 GPa. *J. Phys. Chem. Solids* **2006**, *67*, 1914−1917.
(21) Hromadova, L.; Martonak, R.; Tosatti, E. Structure Change, Layer Sliding, and Metallization in High-Pressure MoS_2. *Phys. Rev. B* **2013**, *87*, 144105−144111.
(22) Sugai, S.; Ueda, T. High-Pressure Raman Spectroscopy in the Layered Materials 2H-MoS_2, 2H-$MoSe_2$, and 2H-$MoTe_2$. *Phys. Rev. B* **1982**, *26* (12), 6554−6558.
(23) Bagnall, A. G.; Liang, W. Y.; Marseglia, E. A.; Welber, B. Raman Studies of MoS_2 at High Pressure. *Phys. B* **1980**, *99*, 343−346.
(24) Hammersley, A. P.; Svensson, S. O.; Hanfland, M.; Fitch, A. N.; Häusermannn, D. Two-Dimensional Detector Software: From Real Detector to Idealized Image or Two-Theta scan. *High Press. Res.* **1996**, *14*, 235−248.
(25) Howard, C. J.; Hunter, B. A. *A Computer Program for Rietveld Analysis of X-ray and Neutron Powder Diffraction Patterns*; Lucas Height Research Laboratories: Sydney, Australia, 1998.
(26) Mao, H. K.; Xu, J.; Bell, P. M. Calibration of the Ruby Pressure Gauge to 800 kbar Under Quasi-Hydrostatic Conditions. *J. Geophys. Res.* **1986**, *91*, 4673−4676.
(27) Bhushan, B. *Modern Tribology Handbook*; CRC Press: Boca Raton, FL, 2000.
(28) Gudelli, V. K.; Kanchana, V.; Appalakondaiah, S.; Vaitheeswaran, G.; Valsakumar, M. C. Phase Stability and Thermoelectric Properties of the Mineral FeS_2: An ab Initio Study. *J. Phys. Chem. C* **2013**, *117* (41), 21120−21131.
(29) Livneh, T.; Sterer, E. Resonant Raman Scattering at Exciton States Tuned by Pressure and Temperature in 2H-MoS_2. *Phys. Rev. B* **2010**, *81*, 195209−195218.